

Article

Effects of Ultrasonic-Aided Quenching on the Corrosion Resistance of GB 35CrMoV Steel in Seawater Environment

Xin Jiang ¹, Yajun Zhou ^{1,2,*}, Chen Shi ^{1,3} and Daheng Mao ¹

¹ College of Mechanical and Electrical Engineering, Central South University, Changsha 410083, China; jiangxin67@csu.edu.cn (X.J.); shichen@csu.edu.cn (C.S.); mdh@csu.edu.cn (D.M.)

² Light Alloy Research Institute, Central South University, Changsha 410083, China

³ National Key Laboratory of High-Performance Complex Manufacturing, Central South University, Changsha 410083, China

* Correspondence: zhouyajun@csu.edu.cn; Tel.: +86-0731-8887-7244

Received: 4 December 2017; Accepted: 30 January 2018; Published: 1 February 2018

Abstract: The effects of ultrasonic-aided quenching (USQ) on the microstructure and corrosion properties of 35CrMoV steel in a simulated seawater environment (wt % (NaCl) = 3.5) were studied. The corrosion properties of the steel were studied by electrochemical impedance spectroscopy (EIS) and potentiodynamic polarization curves. The scanning electron microscope (SEM) and energy dispersive spectrometer (EDS) were used to characterize the microstructure and corrosion products. Combined with the EIS equivalent circuit, the corrosion mechanism was investigated. The results show that the microstructure of the USQ specimen is small martensite and that there was no residual ferrite compared with an un-ultrasonic-aided quenching (UUSQ) sample. It was also found that the corrosion products of USQ sample are less than the UUSQ sample, and the corrosion cracks are lighter and thinner than that of the UUSQ sample, which indicates that the corrosion resistance of 35CrMoV in a seawater environment has been obviously improved.

Keywords: 35CrMoV steel; ultrasonic-aid quenching; microstructure; corrosion resistance; corrosion mechanism

1. Introduction

With the development of science and technology, developing and utilizing marine resources has become an integral part of the national economy, and people have gained much more interest in the use of the ocean than before. However, in the marine environment, steel has a limited service life and high maintenance costs due to corrosion [1–3]. According to the existing data, the corrosion protection cost of metal structures in the general environment covers 2–4% of the total cost, while it accounts for 10–30% in the marine environment. For a 500,000-ton ship, the consumption of steel is as high as 40 tons a year, so protection against corrosion is significant to the development of marine resources.

People are paying more attention than before to ultrasound for its convenience and environmental friendliness. Although the mechanism of its action is not entirely clear until now, many studies show that the technology has wide application prospects. Ultrasonic nanocrystal surface modification (UNSM) has already been used as a treatment for many materials [4–7]. The grain size [4], the properties of wear [5] and fatigue [6] of materials can be markedly improved through UNSM, as it produces surface hardness and compressive residual stress. Ultrasonic welding has also received much attention as an alternative joining technique [7,8]. Barbosa et al. investigated that ultrasonic casting can refine grain size and reduce the porosity shrinkage of the sample [9]. Kessler et al. examined that ultrasonic quenching can improve the mechanical properties of materials by destabilizing the vapor film [10].

However, only a small part of the recent studies have paid attention to the corrosion behavior of steels with ultrasonic treatment. Mordyuk et al. determined that the corrosion resistance can be markedly improved by ultrasonic peening [11].

35CrMoV (Chinese standard) steel belongs to CrMo steel series, a typical mid-carbon steel, which is widely used in the exploration of oceans due to its high static strength, high fatigue limit, and good creep strength. Moreover, its price is far lower than the chromium–nickel steel with the same mechanical properties which is commonly used to replace the large section gear and shaft.

Therefore, the purpose of this paper was to investigate the effects of ultrasonic quenching on the corrosion behavior of 35CrMoV steel in the marine environment. The study will be beneficial for the quenching process of 35CrMoV steel in the seawater environment.

2. Materials and Methods

2.1. Materials

The composition of the 35CrMoV steel is shown in Table 1. Samples were heated up to 850 °C and maintained for 0.5 h with a high-temperature intelligent box furnace (SX2-4-10, Yuandong, Changsha, China), followed by water cooling with and without ultrasonic vibration (Figure 1). The samples were cut into 10 × 10 × 20 mm cubes with a wire cutter machine (DK7735, Guofu, Taizhou, China). The cutting samples were fixed in PC pipes and exposed to an area of 10 × 10 mm for testing.

Table 1. Composition of 35CrMoV steel (wt %).

| Chemical Composition | C | Si | Mn | Cr | Mo | V | S | P | Fe |
|----------------------|------|------|------|------|------|------|-------|-------|------|
| Measured | 0.34 | 0.25 | 0.58 | 1.09 | 0.23 | 0.13 | 0.008 | 0.026 | Bal. |

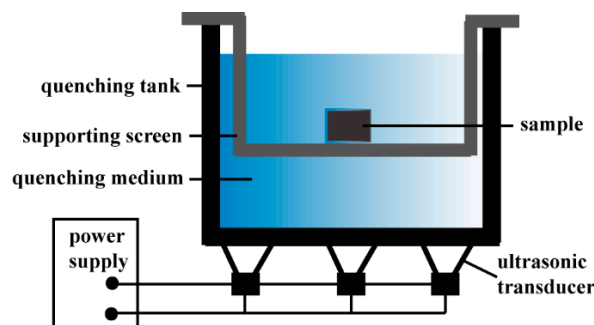


Figure 1. Schematic diagram of quenching.

2.2. Microscopic Analysis

The specimens were wet ground in the sequence of 120, 320, 600, and 1000 grit emery papers and polished with 1 μm diamond suspensions, degreased in ethyl alcohol, rinsed in distilled water, and dried with a stream of hot air. They were then immersed into a nital etchant (2 mL of 70% nitric acid and 48 mL of anhydrous, denatured ethyl alcohol), treated with alcohol swapping, and dried in an air stream. The scanning electron microscope (EVO MA10, ZEISS, Jena, Germany) was used to observe the microstructure of the samples.

2.3. Electrochemical Measurements

The electrochemical experiment was investigated using the electrochemical workstation (Chi660e, Chenhua, Shanghai, China), a traditional three-electrode system (Figure 2). Prior to the tests, samples were wet-ground up to 1000 grit finish and polished with 1 μm diamond suspensions, treated with alcohol swapping, and dried in an air stream. A saturated calomel (Ag/AgCl saturated with KCl) electrode was used as a reference electrode and a platinum piece as a counter electrode. The 35CrMoV samples were used as the working electrode placed in the simulated seawater solution (wt % (NaCl) = 3.5).

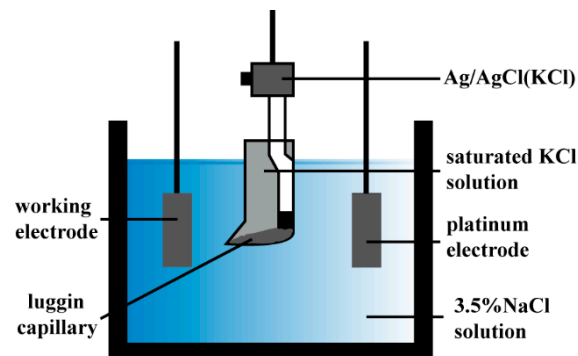


Figure 2. Schematic diagram of three-electrode system.

Before commencing the experiments, the open circuit potential test was applied for 2400 s. The potentiodynamic polarization was scanned at 0.5 mV/s. The electrochemical impedance spectroscopy (EIS) measurements were carried out after 2400 s, at the open circuit potentials, with a range of frequency from 0.1 Hz to 100,000 Hz with an amplitude of 5 mV and a sampling rate of 12 points per decade.

2.4. Corrosion Surface Analysis

The corrosion surfaces of the samples were rinsed with deionized water and ethanol solution and then dried in an air stream. The corrosion morphology, microstructure, and composition of the corrosion products were observed by Phenom scanning electron microscope.

3. Results and Discussion

3.1. Microstructure

As can be seen from Figure 3, the microstructure of the two samples was quite different. The UUSQ sample consisted of a mixture of martensite and residual ferrite, while the USQ sample was all small martensite. This is because 35CrMoV steel belongs to mid-carbon steel. Therefore, if the specimens wanted to cool from the complete austenite temperature to room temperature without high-temperature transformation, the quenching medium must have a higher quenching intensity. Although the water had a certain quenching intensity, some local high-temperature changes still existed during the quenching process. When the ultrasonic wave was added, the hot steam film on the surface of the specimen was ruptured in advance due to its cavitation and sound effect [12]. Therefore, the microstructure of the USQ sample was all small martensite, while the microstructure of the UUSQ sample was bulky martensite and a small amount of residual ferrite.

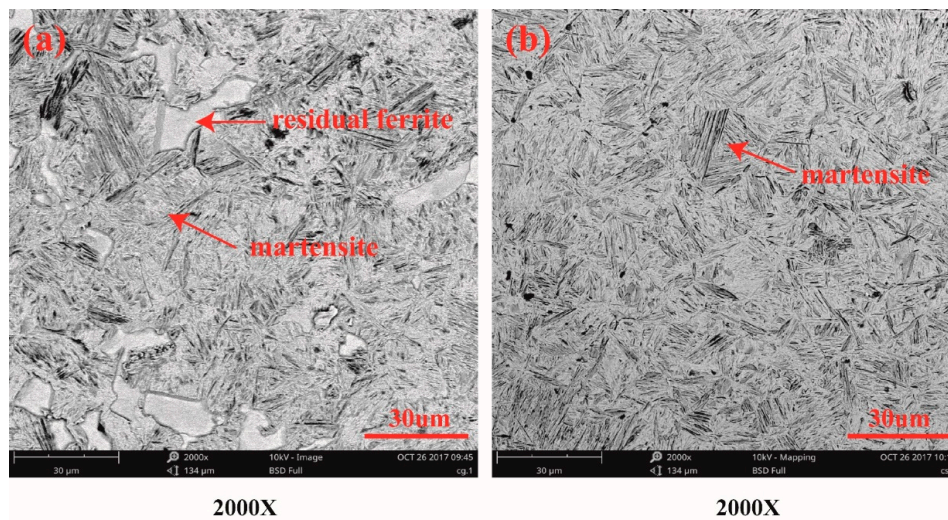


Figure 3. Microstructure of 35CrMoV: (a) un-ultrasonic-aided; (b) ultrasonic-aided.

3.2. Electrochemical Analysis

3.2.1. Electrochemical Impedance Spectroscopy

Figure 4 shows the electrochemical impedance spectroscopy (EIS) results of 35CrMoV in 3.5% NaCl solution. It can be seen from the diagram that the electrochemical impedance spectrum of the two samples was similar in morphology, that is, only an arc of resistance was shown in the entire frequency range of the test, indicating that the electrode reaction is the interface reaction process. Additionally, the semicircular diameter of the USQ sample was significantly larger than that of the UUSQ sample. The semicircular diameter reflects the corrosion resistance of the material, and they are positively related [13]. Thus, the Nyquist curves indicated that the corrosion resistance of the ultrasonic quenching sample was significantly improved.

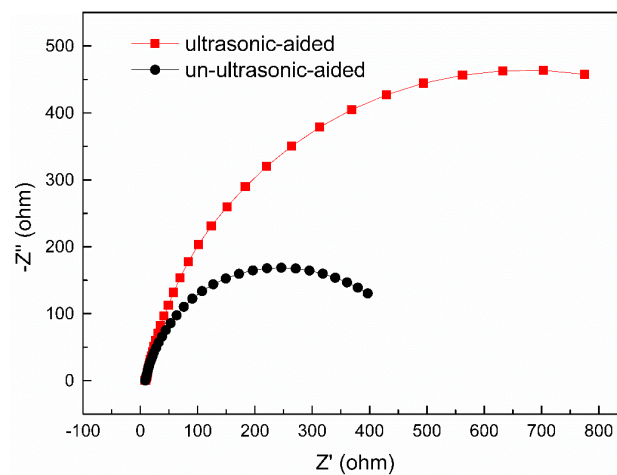


Figure 4. Nyquist EIS spectra of 35CrMoV in artificial seawater solution.

The equivalent circuit model is shown in Figure 5. All the spectra can be well described by the equivalent circuit. This model consists of solution resistance (R_s), charge-transfer resistance (R_{ct}), corrosion products resistance (R_f), and constant phase element (CPE), Q . CPE1 and CPE2 represent

double-layer capacitance of the reaction interface and corrosion products capacitance, respectively. CPE is the constant phase element which contains two parameters [13–15] that can be expressed as:

$$Q - Y_0(j\omega)^n = Y_0\omega^n \cos\left(\frac{n\pi}{2}\right) + jY_0\omega^n \sin\left(\frac{n\pi}{2}\right) \quad (1)$$

where $\omega = 2\pi f$ and f is the frequency in units of Hz. The value of CPE parameter, n varies from 0 to 1. When $n = 1$, the CPE behaves as a pure capacitor, and when $n = 0$, the CPE behaves as a pure resistor. This electrochemical element is best suited to characterize the corrosion mechanism that occurs at the solution or metal interface. The fitting results are shown in Table 2. It was found that the corrosion resistance ($R_p = R_f + R_{ct}$) of the USQ sample was $1513.613 \Omega \cdot \text{cm}^2$, three times as much as $498.88 \Omega \cdot \text{cm}^2$ of the UUSQ sample. This showed that the ultrasonic quenching could obviously improve the corrosion resistance of the sample in the seawater environment, which was consistent with the result of the impedance curve.

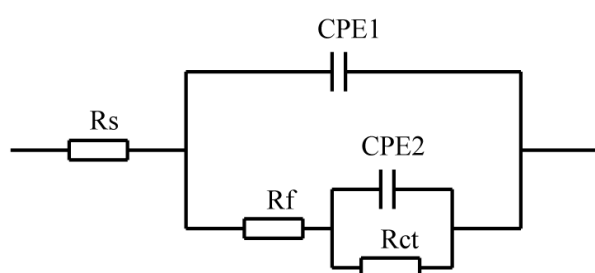


Figure 5. Equivalent circuit model used to fit the EIS data.

Table 2. Fitting parameters calculated by an equivalent circuit.

| Sample | R_s ($\Omega \cdot \text{cm}^2$) | Y_1 ($\Omega \cdot \text{cm}^{-2} \cdot \text{s}^n$) | n | R_f ($\Omega \cdot \text{cm}^2$) | Y_2 ($\Omega \cdot \text{cm}^{-2} \cdot \text{s}^n$) | n | R_{ct} ($\Omega \cdot \text{cm}^2$) |
|---------------------|--------------------------------------|----------------------------------------------------------|--------|--------------------------------------|----------------------------------------------------------|--------|-----------------------------------------|
| Ultrasonic-aided | 7.494 | 2.74×10^{-4} | 0.3255 | 9.613 | 6.795×10^{-4} | 0.8678 | 1504 |
| Un-ultrasonic-aided | 8.621 | 9.07×10^{-4} | 0.8441 | 419.8 | 1.815×10^{-2} | 1 | 79.08 |

3.2.2. Potentiodynamic Polarization Curve

As can be seen from Figure 6, the cathodic currents of the USQ sample and the UUSQ sample, dominantly representing oxygen reduction at -1.0 V were 0.25 mA/cm^2 and 0.61 mA/cm^2 , respectively. The reduction process can be described as [16]



The polarization curves of the two samples were similar, and there were no passivation areas. This was because Cl^- was adsorbed on the surface of the sample and hindered the formation of the passivation film. Combined with Table 3, the corrosion potential of the USQ sample was -651 mV , and the corrosion current density was $6.9 \times 10^{-6} \text{ A} \cdot \text{cm}^{-2}$. Compared with the UUSQ sample, the corrosion potential was increased by 22 mV , and the corrosion current density decreased by several orders of magnitude. According to the electrochemical theory, the corrosion properties of the USQ sample have been improved.

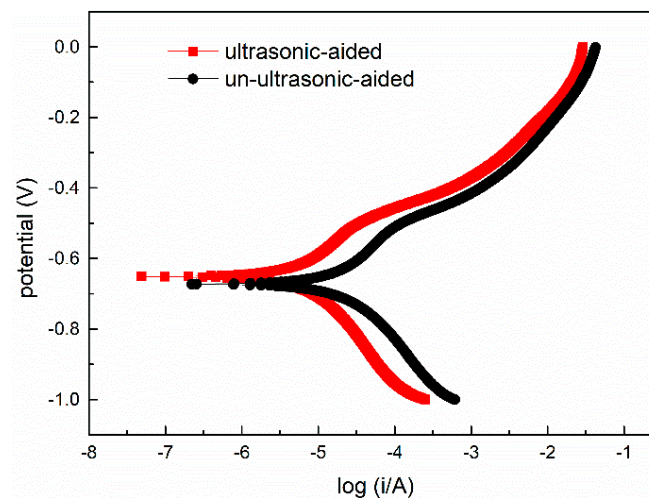


Figure 6. Potentiodynamic polarization curves of 35CrMoV in the artificial seawater solution.

Table 3. Electrochemical test results of 35CrMoV.

| Sample | E_{corr}/V | $R_p/(\Omega \cdot cm^2)$ | $I_{corr}/(A \cdot cm^{-2})$ | $ba/(V/Decade)$ | $bc/(V/Decade)$ |
|---------------------|--------------|---------------------------|------------------------------|-----------------|-----------------|
| Ultrasonic-aided | -0.651 | 5947.6 | 6.91×10^{-6} | 0.054 | 0.051 |
| Un-ultrasonic-aided | -0.673 | 1954.0 | 2.085×10^{-5} | 0.050 | 0.056 |

3.3. Corrosion Products and Corrosion Mechanism Analysis

It can be seen from Figure 7 that the cracks were all over the surface after dehydration and the corrosion products on the surface started along the grain boundary. This was typical intergranular corrosion. Because the activity of grain boundary was relatively large, so the corrosion process began at or near the grain boundary first [17]. Furthermore, the corrosion products of the USQ sample were attached to the surface, while the corrosion products of the local area of the UUSQ sample had fallen off, and pitting occurred (Figure 7b,e). Additionally, the corrosion cracks of the UUSQ sample were much wider, deeper, and denser than that of the USQ sample (Figure 7c,f). This was because the grains of the carbides of steel obtained by UUSQ were big and unevenly distributed in the microstructure [18,19]. While under the effect of ultrasound, the cooling speed of the sample was greater than the critical cooling rate, which can obtain more uniformly distributed, fine-grained, and regularly shaped carbides to help steel improve the corrosion resistance. In other words, the corrosion resistance of the USQ sample was better than that of the UUSQ sample in seawater environment. The same conclusion can be obtained from the electrochemical test analysis.

Figure 8 shows the corroded surface microstructure and EDS analysis of 35CrMoV. It can be observed that the corrosion layer has been seriously damaged. At the same time, the agglomerated-like corrosion products can be seen in the corrosion cracking area. In combination with Figure 8 and Table 1, it is not difficult to see that the corrosion products of the samples are mainly composed of C, O, and Fe elements. We can speculate that the activation of erosion due to the Cl^- adsorbed on the metal surface, and Fe^{2+} dissolved from the anode, unites with Cl^- to form $FeCl_2 \cdot 4H_2O$, and then generate $Fe(OH)_2$. However, the $Fe(OH)_2$ was not stable, and would gradually break down into FeO or combine with O_2 in water to form $FeOOH$ [16,20,21]. Finally, the oxygen content of the UUSQ sample is significantly increased compared with USQ sample, indicating that ultrasonic quenching can improve the corrosion resistance of steel in a seawater environment.

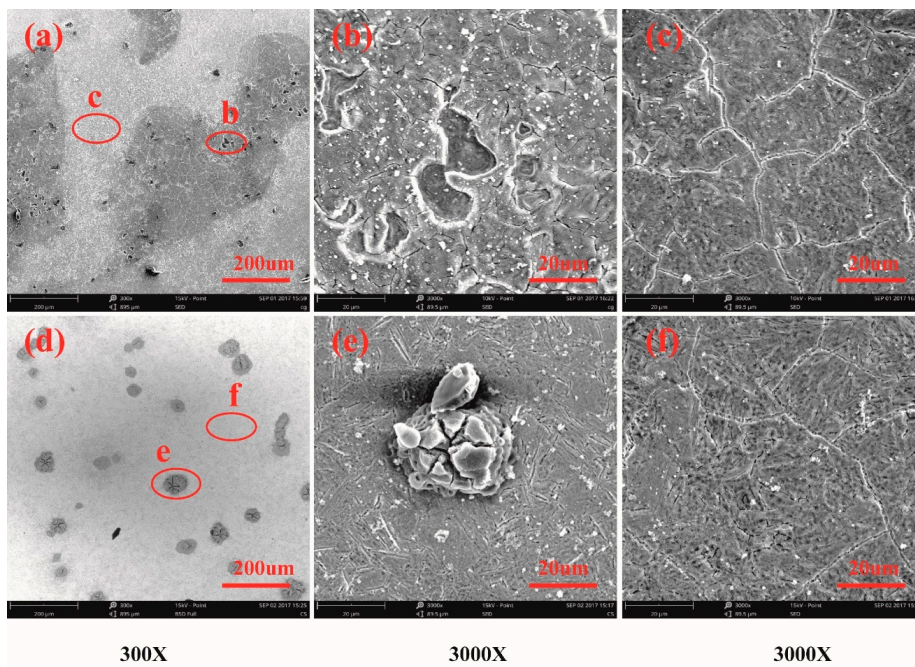


Figure 7. SEM images of the 35CrMoV corrosion surface: (a–c) un-ultrasonic-aided; (d–f) ultrasonic-aided.

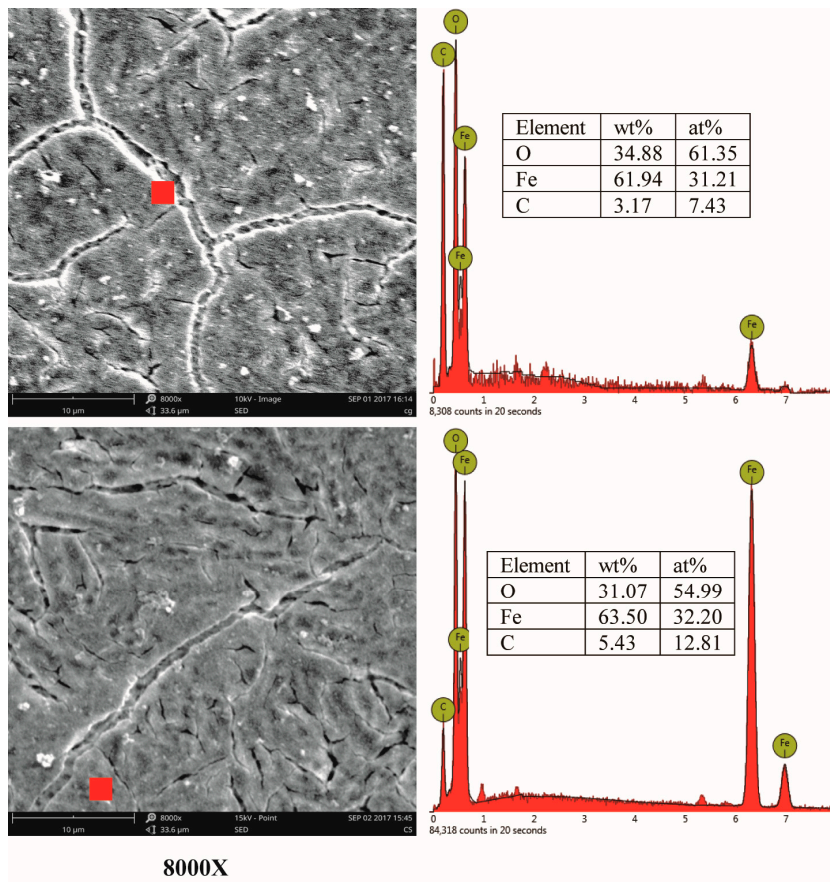


Figure 8. Surface corrosion morphology and EDS spectrum analysis of 35CrMoV corrosion surface: (a) un-ultrasonic-aided; (b) ultrasonic-aided.

4. Conclusions

The effects of USQ on 35CrMoV steel corrosion in a seawater environment were investigated by SEM, EDS, and EIS.

1. Ultrasonic waves can increase the quenching intensity of the quenching medium, and helped to reduce residual ferrite and refine the martensite in 35CrMoV steel.
2. Compared with the UUSQ sample, the corrosion potential of the USQ sample increased, and the corrosion current density decreased by several orders of magnitude.
3. The corrosion cracks of the UUSQ sample were much wider, deeper, and denser than that of the USQ sample, verifying that the USQ sample had a better corrosion resistance in a seawater environment.

Acknowledgments: The authors would like to acknowledge the financial assistance provided by Major State Basic Research Development Program of China (No. 2014CB046702).

Author Contributions: Xin Jiang and Yajun Zhou conceived of and designed the experiments; Xin Jiang carried out the experiments; Xin Jiang, Yajun Zhou, and Chen Shi analyzed the data; Daheng Mao contributed reagents, materials, and analysis tools; and Xin Jiang wrote the paper.

Conflicts of Interest: The authors declare no conflict of interest.

References

1. Liu, Y.D.; Zhou, Y.; Xiao-Lin, M.A. Corrosion Behaviors of Several Kinds of Arc Sprayed Metal Coatings in 3.5%NaCl Solution. *Surf. Technol.* **2016**, *45*, 71–75.
2. Hossain, K.M.A.; Easa, S.M.; Lachemi, M. Evaluation of the effect of marine salts on urban built infrastructure. *Built. Environ.* **2009**, *44*, 713–722. [[CrossRef](#)]
3. Meng, H.; Hu, X.; Neville, A. A systematic erosion-corrosion study of two stainless steels in marine conditions via experimental design. *Wear* **2007**, *263*, 355–362. [[CrossRef](#)]
4. Wu, X.; Tao, N.; Hong, Y.; Xu, B.; Lu, J.; Lu, K. Microstructure and evolution of mechanically-induced ultrafine grain in surface layer of AL-alloy subjected to USSP. *Acta Mater.* **2002**, *50*, 2075–2084. [[CrossRef](#)]
5. Amanov, A.; Penkov, O.V.; Pyun, Y.; Kim, D. Effects of ultrasonic nanocrystalline surface modification on the tribological properties of AZ91D magnesium alloy. *Tribol. Int.* **2012**, *54*, 106–113. [[CrossRef](#)]
6. Wu, B.; Zhang, J.; Zhang, L.; Pyoun, Y.; Murakami, R. Effect of ultrasonic nanocrystal surface modification on surface and fatigue properties of quenching and tempering S45C steel. *Appl. Surf. Sci.* **2014**, *321*, 318–330. [[CrossRef](#)]
7. Matsuoka, S.; Imai, H. Direct welding of different metals used ultrasonic vibration. *J. Mater. Process. Technol.* **2009**, *209*, 954–960. [[CrossRef](#)]
8. Yang, J.; Cao, B. Investigation of resistance heat assisted ultrasonic welding of 6061 aluminum alloys to pure copper. *Mater. Des.* **2015**, *74*, 19–24. [[CrossRef](#)]
9. Barbosa, J.; Puga, H. Ultrasonic melt processing in the low pressure investment casting of Al alloys. *J. Mater. Process. Technol.* **2017**, *244*, 150–156. [[CrossRef](#)]
10. Kessler, R.R.O. Ultrasonic assisted water quenching of aluminium and steel cylinders. *Int. Heat Treat. Surf. Eng.* **2013**, *2013*, 115–121.
11. Mordyuk, B.N.; Prokopenk, G.I.; Vasylyev, M.A.; Iefimov, M.O. Effect of structure evolution induced by ultrasonic peening on the corrosion behavior of AISI-321 stainless steel. *Mater. Sci. Eng. A* **2007**, *458*, 253–261. [[CrossRef](#)]
12. Komarov, S. Cavitation Phenomena in Ultrasonic Casting and Their Industrial Application. *Tetsu-to-Hagane* **2016**, *102*, 179–185. [[CrossRef](#)]
13. Chen, Y.; Orazem, M.E. Impedance analysis of ASTM A416 tendon steel corrosion in alkaline simulated pore solutions. *Corros. Sci.* **2016**, *104*, 26–35. [[CrossRef](#)]
14. Jorcin, J.B.; Orazem, M.E.; Pebere, N.; Tribollet, B. CPE analysis by local electrochemical impedance spectroscopy. *Electrochim. Acta* **2006**, *51*, 1473–1479. [[CrossRef](#)]

15. Hirschorn, B.; Orazem, M.E.; Tribollet, B.; Vivier, V.; Frateur, I.; Musiani, M. Determination of effective capacitance and film thickness from constant-phase-element parameters. *Electrochim. Acta* **2010**, *55*, 6218–6227. [[CrossRef](#)]
16. Eliyan, F.F.; Alfantazi, A. Corrosion of the Heat-Affected Zones (HAZs) of API-X100 pipeline steel in dilute bicarbonate solutions at 90 °C—An electrochemical evaluation. *Corros. Sci.* **2013**, *74*, 297–307. [[CrossRef](#)]
17. Ping, H.; Rui, S.; Kuaishe, W.; Fan, Y.; Boliang, H.; Yu, C.Z. Electrochemical Corrosion Behavior of Titanium-Zirconium-Molybdenum Alloy. *Rare Metal Mater. Eng.* **2017**, *46*, 1225–1230. [[CrossRef](#)]
18. Lei, L.; Liang, Y.; Jiang, Y. Effect of Quench Rate on the High Cycle Fatigue Property of 60Si2CrVAT Spring Steels. *Trans. Mater. Heat Treat.* **2017**, *31*, 65–73.
19. Huang, X.L.; He, Y.H.; Zhang, Q.; Shen, W.; Zhang, H. Effect of heat treatment on the structure and mechanical properties of 18%Cr martensitic stainless steel. *Mater. Sci. Eng. Powder Metall.* **2017**, *22*, 503–509.
20. Hao, X.C.; Su, P.; Xiao, K. Influence of NaCl Concentration on Corrosion Products of Weathering Steel. *Corros. Prot.* **2009**, *30*, 297–299.
21. Kimura, M.; Kihira, H.; Ohta, N.; Hashimoto, M.; Senuma, T. Control of Fe(O,OH)₆ nano-network structures of rust for high atmospheric-corrosion resistance. *Corros. Sci.* **2005**, *47*, 2499–2509. [[CrossRef](#)]



© 2018 by the authors. Licensee MDPI, Basel, Switzerland. This article is an open access article distributed under the terms and conditions of the Creative Commons Attribution (CC BY) license (<http://creativecommons.org/licenses/by/4.0/>).